Published in final edited form as:
Small. 2008 August ; 4(8): 1183–1195. doi:10.1002/smll.200701290.

Scalable routes to gold nanoshells with tunable sizes and their response to near infrared pulsed laser irradiation

Brian G. Prevo and **Shelley A. Esakoff**
Department of Chemical Engineering, University of California, Santa Barbara Santa Barbara, California 93106-5080

Alexander Mikhailovsky
Department of Chemistry University of California, Santa Barbara Santa Barbara, California 93106-5080

Joseph A. Zasadzinski[*]
Department of Chemical Engineering, University of California, Santa Barbara Santa Barbara, California 93106-5080

Abstract

We present a simplified synthesis of hollow gold nanoshells 20-50 nm in diameter via the well-established templated galvanic replacement reaction of silver for gold. The surface plasmon resonance absorbance of nanoshells made in this fashion can be tuned using basic colloid chemistry to control the size of the silver templates. The gold nanoshells can be varied in size and shell thickness depending on silver/gold reagent ratios and have an aqueous core. The template replacement chemistry is rapid, highly scalable, uses minimal amounts of toxic reagents, and in many cases is a true `one pot' synthesis. The smallest nanoshells (20 nm diameter, 7 nm wall thickness) reach the highest temperature on irradiation with femtosecond light pulses in the near infrared and anneal to form spherical nanoparticles fastest, even though their plasmon resonance does not overlap as well as the larger nanoshells (50 nm diameter, 7 nm wall thickness) with the 800 nm wavelength excitation. Optimizing a nanoshell structure to reach the highest nanoshell temperature is not the same as optimizing the structure for maximum energy absorbance.

Keywords

Nanoparticles; galvanic replacement reactions; silver

1. Introduction

Physiological media (water, blood, and tissue) are relatively transparent in the near infrared (NIR) region of the spectrum, allowing tissue penetration depths of up to 10 centimeters [1]. In the past decade, a variety of nanoscale materials that have high absorption cross sections in the near-infrared have been developed [2-13]. The most readily adapted to biomedical applications are gold nanoparticles [14-16], core/shell nanoparticles (colloidal scale dielectric core / gold shell particles) [3,4,6,7,17-24], hollow core nanoshells, [12,25-34] or gold nanorods [2,10,11,13,35-39], which adsorb strongly in the NIR, are sufficiently small to enable long circulation times *in vivo* [40], and are chemically inert and non-toxic [14]. Because gold nanoparticles strongly absorb NIR light, photothermal energy conversion using pulsed laser

*To whom correspondence should be addressed..

irradiation can be used to locally heat nanoscale volumes without heating the bulk of the solution volume [2,15,16,23,35,36,41-44]. Such phenomena are commonly referred to as photothermal heating or plasmonic heating, [3,10] and can be used to induce drug release from polymers, [20,45,46] or induce localized hyperthermia to kill cancer or bacterial cells [3,6, 12,13,16,37,47]. Local plasmonic heating with gold nanoshells has also recently been used to denature proteins used in `stitchless' laser wound closure [7]. However, in these applications, it is not obvious if the suspension should be optimized for maximum nanoshell temperature or maximum nanoshell energy absorption.

One of the first methods of nanoshell fabrication was a core-shell method pioneered by Halas and coworkers [8,19,21,48] in which a dielectric core particle (typically silica, although polystyrene [24] has also been used) surface is first decorated with gold-binding ligands, followed by covalent linkage of gold nanoparticles that act as nucleation sites. The shell is completed via additional gold reduction in solution at the nanoparticle nucleation sites. The plasmon adsorption of the silica/gold core/shell nanoparticles can be tuned by varying the ratio of the gold shell thickness to the shell radius [8,19-24,48,49]. Layer-by-layer self-assembly has also been used to construct core/shell composite colloidal architectures by adsorbing oppositely charged polyelectrolytes to a core particle and then adsorbing the charged gold colloids to make up the shell [45,46]. While these multilayer dielectric/gold core/shell approaches have demonstrated potential [21], one major limitation is the time and labor required for fabrication [25]. Each step to the core-shell nanoparticle must be accompanied by a centrifugation and rinsing step, which can reduce the yield and more importantly, destabilize the colloidal particles and lead to irreversible aggregation. For the layer-by-layer assemblies, the sizes are usually in the 1 - 10 micron range [45,46], which limits the biomedical applications [40].

Xia and coworkers developed templated galvanic replacement reactions and have shown that many different kinds of shape anisotropic silver nanoparticles can be used to generate hollow gold nanoshell morphologies that exhibit different surface plasmon resonance phenomena spread across the NIR region of the spectrum [12,25,28,29,50]. However, many of the chemical approaches use materials that are incompatible with biomedical applications. Alternatively, good control can be achieved over the morphology of gold nanoshells made via galvanic replacement at ambient temperatures by employing a cobalt template route [34], but the sensitivity to atmospheric oxygen in this process requires that the reactions be performed under a nitrogen blanket, and cobalt can be toxic and should be avoided for biomedical applications.

We have taken advantage of these templated galvanic replacement reactions of silver for gold [25,27,31,33,50] to create a simple and reproducible route to gold nanoshells 20-50 nm in diameter for use in biomedical applications. As in previous templated galvanic replacement methods [12,25,27-29,34,50], the core particle is sacrificed; the metal salt that makes up the nanoshell is reduced to metal if it has a greater standard reduction potential than the template metal, which is oxidized to a molecular solution [25]. The size and surface plasmon resonance (SPR) absorbance of nanoshells made in this fashion can be tuned very simply by applying Turkevich's basic colloidal growth chemistry to the sacrificial silver sols [51-54]. The emphasis here is not on making shape specific or extremely monodisperse nanoshells, but rather on a simple and scalable route to nanoshells for practical applications with tunable sizes and absorbance profiles that require minimal experimental footprints (reduced heating, etc.) and minimal exposure to toxic reagents or intermediates that would be detrimental to biomedical applications. The major benefit of this new synthesis is that it is rapid, stable, highly scalable, and in many cases is a true `one pot' synthesis [33,50].

This simple synthesis gives nanoshells that have strong absorbances across the NIR window. Femtosecond NIR light pulses can heat these nanoshells sufficiently to melt and/or ablate the

nanoshells into smaller nanoparticles, with an accompanying shift in the plasmon absorbance, which makes them suitable for applications in plasmonic heating [23]. The more unexpected result is that the maximum temperature of the individual nanoshells is governed by a competition between the red-shift of the SPR peak (which increases the overlap with the NIR irradiation), which increases with the nanoshell diameter to shell thickness ratio, and the increased mass of the nanoshells (which increases roughly as the square of the nanoshell diameter). Optimizing the nanoshell structure for maximum light absorption in the NIR does not necessarily provide the highest maximum temperatures for the individual nanoshells during pulsed irradiation; however, it is not yet known which is most important for biomedical applications such as photothermal destruction of cancer or bacterial cells [3,6,7,12,13,15,16, 23,46,47,55]. Conversely, nanoparticles heated by continuous wave laser irradiation dissipate the absorbed energy into the surrounding environment without substantial increases in nanoparticle temperature [43,56]. Hence, maximum energy absorption is the only relevant feature, which has led previous efforts to tailor the nanoparticle absorption to the irradiation wavelength.

2. Results

Stable suspensions of silver nanoparticles were synthesized in minutes using sodium citrate and silver nitrate. The addition of sodium borohydride accelerates the chemical reactions, and the resulting nanoparticles are ~ 15-25 nm in diameter. Larger silver particles can be formed from these nanoparticles by reducing additional silver nitrate in the presence of hydroxylamine hydrochloride; the nanoparticles act as nuclei for further growth [51-54]. Hydroxylamine hydrochloride is a `gentle' reducing agent, and does not induce secondary nucleation of new silver particles [51]. The total absorbance at the 400 nm peak associated with the plasmon resonance of silver nanoparticles increased with increased silver nitrate concentration. There was a slight red-shift in the SPR peak as the particles grew, but was much less pronounced than that observed for gold nanoparticles [52,54,57,58].

Figure 1 shows that on a log-log scale, that the average hydrodynamic radius measured by dynamic light scattering (DLS) increased linearly from the initial 28 nm of the original 0.2 mmol stock sol with increasing silver nitrate concentration. The 1/3 slope of the line through the data, (the origin of which was set to the initial average diameter of 28 nm as measured by DLS), consistent with the bulk of the added silver being added to existing nanoparticles with a minimum of new nucleation as given by a simple mass balance [51]:

$$\frac{D_f}{D_i}=\left(\frac{A_n+A_g}{A_n}\right)^{1/3} \quad (1)$$

in which D_f is the final nanoparticle diameter, D_n is the diameter of the initial silver nuclei, A_n is the silver nitrate concentration needed to grow the nuclei, and A_g is the added silver nitrate needed to grow the particles. Hence, the increase in absorbance in Fig. 1a is due to the increase in total silver concentration at a constant overall particle concentration.

The silver nanoparticles were converted into gold nanoshells by adding $HAuCl_4$ directly to the as-grown nanoparticle solution, with no centrifugation or rinsing steps. Silver (Ag^+/Ag 0.8V, vs SHE) has a lower redox potential than does gold ($AuCl_4^-/Au$ 0.99V, vs SHE) and the replacement reaction is [25]:

$$3Ag_{(s)}+AuCl^-_{4\,(aq)} \rightarrow Au_{(s)}+3Ag^+_{(aq)}+4Cl^-_{(aq)}$$

Upon the addition of the concentrated $HAuCl_4$, the solution turns from yellow/orange to grey/yellow to blue/grey to blue/turquoise within seconds as the silver and gold were oxidized and reduced, respectively. The process was complete in a few minutes according to the UV/vis spectra, but the reaction mixture was stirred for an additional hour, then refrigerated at 4°C.

Figure 2a shows the evolution of the UV-NIR spectra as different amounts of $HAuCl_4$ were added to the silver nanoparticles grown from the original 0.2 mmol $AgNO_3$ stock sol. The gold peak gradually red-shifts during the reaction from 400 nm to about 620 nm. This is consistent with independent nucleation and growth of the gold nanoshells around the dissolving silver template until the shell knits together and is complete, giving the final surface plasmon resonance. However, the point where the silver peak and the gold peak cross is at nearly the same wavelength and intensity throughout the reaction. This transition point is referred to as an isosbestic point [26], and is indicative of a direct transition between two states (in this case between metallic silver and gold). If there were intermediate states, these would manifest themselves as additional peaks between the initial and final peaks. Regardless of the initial silver template size, gold nanoshell formation is direct and there is little secondary nucleation of gold nanoparticles, otherwise an SPR peak located near 520 nm (indicative of solid gold nanoparticles [52]) would appear. The final ratio of added gold to silver was always slightly greater than 1/3 to insure that the reaction went to completion (0.37 - .38:1).

Increasing amounts of gold were required to form the shells around the larger silver template cores. The same 0.2 mmol stock silver sol was used in all cases (10^{10} - 10^{11} particles-mL^{-1}), so the particle concentration is approximately the same regardless of the final silver nanoparticle size. The magnitude of the gold surface plasmon resonance is concentration dependent (Fig. 2b), and follows a shift to longer wavelengths, which is expected from nanoshells with roughly constant wall thickness, but increasing diameter as predicted by Mie theory calculations of the extinction behavior [47,52] (Figure 2c). The wavelength of the SPR increases with the initial silver concentration (which is also a measure of the initial particle size or relative ratio of shell to diameter, See Fig. 1b), providing a rough guide to tuning the SPR absorbance maximum across the NIR region (Fig. 2d). A macroscopic view of the gold nanoshells (some which have spectra plotted in Fig. 2b) is shown in Figure 2e demonstrating the characteristic change in color with increasing silver template size [52].

Representative TEM images of the particle suspensions are shown in Figure 3. From these images, it is clear that the gold particles are hollow shells and that the size of the nanoshells depends on the size of the silver template. X-ray photoelectron spectroscopy (XPS) verified that silver was present with the gold metal after the galvanic replacement took place, but not the chemical state, Ag^{+1} or Ag^0, of the silver. The silver signature was present even after the samples had been dialyzed in 5mmol citrate solutions for several days, indicating that the silver was likely insoluble and associated with the nanoshells [12]. For our purposes, attaining tunable SPR frequencies in NIR window for sub 100 nm gold particles is sufficient; any residual silver will not negatively impact applications. In fact, Ag^0 or Ag^{+1} have antimicrobial properties and their presence may provide additional benefits to the sol [59].

The SPR peak of the gold nanoshells can be readily tuned from 600 - 800nm simply by adjusting the amount of initial silver present in the silver growth sol. The SPR resonance of the gold nanoshells made from silver nanoparticles plateaus around 800nm, with no further increase with increasing silver particle size. This is likely because significant settling occurs for metal nanoparticles >100 nm, which can detract from the diffusion limited reaction conditions. The use of additional citrate stabilizing agent, or rapid post reaction steric stabilization using polyethylene glycol - thiol (PEG-SH) or gelatin [52] may contribute greater stability to these larger particles and allow tuning further into the NIR, although this does not appear to be necessary for plasmonic heating applications.

2.1 The effect of NIR laser irradiation upon hollow gold nanoshells

The citrate and sodium borohydride reduced (golden yellow colored) silver nanoparticles used for these studies were stable for months. It is well-established that silver and gold nanoparticles made via similar chemistries are metastable against aggregation for years [51,52,60]. The particles are stabilized against flocculation by residual ions adsorbed to the particle surfaces (e.g. citrate and or BO_2^- ions), imparting a net negative surface charge [60]. The gold nanoshells made via silver template particles were stable for many weeks or months, thus it is likely that they have also adsorbed charged species that provide electrostatic stability. The surface charge of these particles is negative, as they tightly adhere to positively charged surfaces. Thus, they are more likely retaining the original charged groups from the template particles, and if any settling did occur, brief sonication was sufficient to re-suspend the particles.

The gold nanoshell suspensions remain their original color (the actual color varied with composition or size of the particles, See Fig. 2e) after short periods of irradiation at 800 nm. However, with increased total energy input, the gold nanoparticle sols eventually turned reddish in color, indicating a change in the particle morphology. After irradiation, the nanoshell suspensions were less stable, settling occurred within 24 hours of irradiation (regardless of the energy level used). Particles could be re-suspended by sonication, but several repetitions of settling and re-dispersing revealed the onset of visible dark flocs (indicating irreversible aggregation). Similar observations of accelerated aggregation of solid gold nanoparticles in the presence of laser irradiation have been reported in the literature [61].

Figure 4 shows the changes in the UV/visible/NIR spectra after 10 minutes of various laser irradiation intensities for different sized gold nanoshells formed from the various silver templates: 0.2 mmol Ag (20 nm diameter nanoshells formed after addition of 0.09 mmol Au, SPR ~ 600 nm), 0.304 mmol Ag (30 nm diameter nanoshells, 0.124 mmol Au, SPR ~ 650nm), 0.675 mmol Ag (40 nm diameter nanoshells, 0.25 mmol Au, SPR ~720nm), and 1.07 mmol Ag (50 nm diameter nanoshells, 0.42 mmol Au, SPR ~750nm) after irradiation. The smaller particles (SPR < 700 nm) exhibit a monotonic shift to shorter wavelengths in response to the laser irradiation (Figs. 4a, b). This indicates an almost immediate elimination of complete nanoshells. After irradiation, the peak maximum settles between 500 - 550 nm, consistent with the expected absorbance of 10 - 40 nm solid, spherical nanoparticles (See TEM images in Fig. 5).

The spectra of the larger particles (Fig. 4c, d) first exhibited a red-shift to longer wavelengths upon irradiation at low intensity; new peaks appeared at longer wavelengths (~ 900 nm) that had lower magnitudes than the original SPR peak (indicating lower concentrations). Prior to irradiation, these larger gold nanoshells were more polydisperse, and exhibited broader SPR peaks than their smaller counterparts (See Figs. 2b, c). Eventually, the SPR peak shifted to wavelengths between 500 - 600 nm at maximum laser power as in Figs. 4a, b (~ 700 $\mu J\text{-}pulse^{-1}$); again indicating that smaller spherical particles were being formed due to the plasmon heating. This process is sometimes referred to as `hole burning,' [2, 42], in which a portion of an absorption peak is removed via direct irradiation at that wavelength. The broad SPR of the un-irradiated sols is likely a summation of the different resonances of nanoshells that are polydisperse in both shape and size (see Figs. 3, 5). However, the SPR peak near 800 nm decreased rapidly upon laser irradiation (hole burning) as those particles responsible for the 800 nm peak melted and were reduced in size, revealing other absorbance peaks that were present before irradiation (at lower intensities, due to the lower concentration of nanoparticles with resonances at these other wavelengths). The apparent transition to longer wavelengths has been observed in other systems including gold nanorods, which can have an axial SPR in the NIR window [2, 42]. As the laser energies increase, all particle populations melt [44] and shift their SPR to 500 - 600 nm consistent with the transition to solid spherical nanoparticles.

Figure 5 shows TEM images of the evolution of the nanoshells after 10 minutes of irradiation with 800 nm light pulses of either 350 or 700 μJ energy. After irradiation at 700 μJ, all of the nanoshells, regardless of initial size, appear to have sintered and annealed into solid, spherical particles [2,44]. There was a collapse of the hollow core, sometimes leaving a small residual hollow within the melted particle. However, images at 350 μJ show that instead of simply collapsing to form smaller, solid spherical nanoparticles, the larger nanoshells sometimes break apart upon absorbing the photon energy, leading to a disperse collection of asymmetric incomplete shells, oblate spheroids, rods and branched structures such that several different SPR resonances likely result [39,42]. The elimination of the 800 nm peak seen in Figs. 4c,d may be the result of these changes in particle shapes. [42] However, the images of the nanoshells exposed to the highest laser power show that all the nanoshells examined reach the melting point of gold (> 1064 °C) and eventually condense into solid spherical nanoparticles of 10 - 40 nm diameter.

Fig. 6 shows the absorption kinetics of the nanoshells which were followed by measuring the light transmitted through the sample; whatever light is not transmitted is absorbed by the nanoshells or scattered (see Fig. 7). In Fig. 6a, irradiation of 20 nm diameter nanoshells (0.098 mmol Au) with a SPR ~ 600 nm show a rapid increase from about 50% transmission to 75-80% transmission within 1 minute for all of the incident light pulse energies. The transmitted energy is then almost constant suggesting that the particles are no longer changing shape, which means that the absorption due to the SPR is constant as well.

In Fig. 6c, for 40 nm diameter nanoshells (~ .25 mmol Au) with an SPR closer to the 800 nm wavelength of the laser (See Fig. 2b, 4), the fraction of laser power transmitted through the sample depends much more on the pulse energy. Consistent with the SPR absorption peak overlapping the incident light wavelength, the initial transmission was close to zero. For a pulse energy of 161 μJ, the transmitted intensity increases only to about 25 μJ after 10 minutes; only 16% of the incident energy was transmitted. In comparison, for a pulse energy of 700 μJ, 410 μJ or ~ 60% of the incident energy was transmitted after 10 minutes. These differences in transmitted intensity with time are likely due to different changes in the nanoshell morphology (Fig. 5) that lead to the changes in nanoshell absorption as shown in Figure 4. With increasing laser pulse energy, Fig. 5 shows that all of the nanoshells eventually melt and anneal into more stable solid nanoparticles with less adsorption at 800 nm. For smaller irradiation energy, the larger nanoshells break up to form shapes with new absorption peaks that still absorb a substantial fraction of the incident light. The larger particles apparently take more time to anneal into the final spherical gold particles that are the stable form after irradiation. Fig. 6d summarizes the kinetics of the change in transmission for the highest pulse energy of 680 μJ with the gold concentration, and hence the size and SPR of the gold nanoshells. The largest particles anneal more slowly than the smaller particles, even though the nanoshell SPR peak overlaps more with the incident 800 nm wavelength light. Only 44% of the incident light is transmitted through the sample with the 50 nm nanoshells (0.42 mmol Au) compared to the 81% transmission through the 20 nm nanoshells (0.098 mmol Au) after 10 minutes of irradiation.

3. Discussion

The kinetics suggest that the smaller nanoshells anneal more quickly than do the larger nanoshells, even though more total energy is absorbed by the larger nanoshells. From the known particle absorbance and concentration, a simple energy balance incorporating Beer's law can be used to determine the energy per gram of gold, Q (J/g), that the nanoshells of various sizes absorb during a given NIR laser pulse [43]:

$$Q=\frac{I_0(1-\xi)^2\left(1-10^{-A}\right)\varepsilon_A}{[Au]\sigma l} \quad (2)$$

A is the absorbance ($-\log_{10}$ of the transmitted light), [Au] is the gold mass concentration in the sol, σ is the Gaussian beam area (0.042 cm^2), l is the laser path length through the cuvette (1 cm), $I_0(1-\xi)^2$ is the incident laser intensity adjusted for reflectance losses from the cuvette/air interfaces ($(1-\xi)^2 \sim 0.9$ for all of the cuvettes used), and ε_A is the relative absorption efficiency of the gold nanoshells (a measure of how much of the non-transmitted light is absorbed rather than scattered). The energy absorbed per nanoshell per pulse is $Q_{abs} = \rho_g VQ$, in which ρ_g is the density of gold (19.32 g-cm^{-3}) and V is the volume of gold in the nanoshell (in cm^3). Figure 7 shows Mie calculations for the extinction, scattering and adsorption efficiencies for 30 and 50 nm diameter cores with 7 nm thick shells. The ratio of the absorption efficiency to the extinction efficiency gives an estimate of the relative absorption efficiency, ε_A. $\varepsilon_A \sim 0.95$ for 30 nm diameter nanoshells with a 7 nm wall thickness and ε_A decreases to ~ 0.8 for 50 nm diameter nanoshells with a 7 nm wall thickness. As the particle sizes increases, scattering increases and the relative absorption efficiency decreases, although this is partially compensated by the stronger overlap of the larger nanoshells with the irradiation laser wavelength of 800 nm.

From the spectroscopy and TEM images, it is apparent that the shape and sizes of the nanoshells are significantly altered by irradiation, implying a large rise in nanoshell temperature. From the estimate of the energy absorbed per particle from Eqn. 2, the temperature reached by the gold nanoshells during a light pulse can be calculated if heat transfer to the surrounding solution is slow in comparison to the plasmonic heating [43,44]. To determine the temperatures reached by the nanoshells, it is necessary to consider if the irradiation energy per gram, Q, is sufficient to heat the nanoshell to the melting temperature of gold, T_m (1064°C is the bulk melting point of gold). For nanometer dimension particles, the melting temperature of spherical gold particles decreases with decreasing size [62], but the effect is minimal for particles greater than 20 nm in diameter. If, $Q \leq C_{pg}(T_m - T_i)$ (C_{pg} is the heat capacity of gold (.129 J-g^{-1}-K^{-1}), taken to be constant for liquid or solid phases and T_i is the initial temperature of the nanoshell, ~135 J-g^{-1} is required to reach the melting point of gold from 20 °C), then

$$T=T_i+\frac{Q}{C_{pg}}. \quad (3a)$$

If the nanoshell reaches the gold melting temperature (which may be slightly suppressed due to the nanometer scale dimensions of the particles [62]), the enthalpy associated with melting the gold, ΔH_{Melt} (64 J-g^{-1}) must be supplied before further increase in temperature occurs: that is, $T=T_m$ for

$$C_{pg}(T_m - T_i) + Q + C_{pg}(T_m - T_i) + \Delta H_{melt}; \quad (3b)$$

so $T=T_m$ for 135 J-g^{-1} < Q< 199 J-g^{-1}. For Q > 199 J-g^{-1}:

$$T=T_i+\frac{Q-\Delta H_{melt}}{C_{pg}} \quad (3c)$$

Finally, if the temperature of vaporization of gold is reached (2856 °C, Q > 430 J-g^{-1}), then the enthalpy associated with gold vaporization, $\Delta H_{Vap,}$ (1870 J-g^{-1}) must be supplied before any further increase in temperature occurs.

From Eqn. 2, the energy associated with light adsorption can be estimated and set equal to the appropriate version of Eqn. 3, depending on the magnitude of the adsorption energy, to determine the maximum nanoshell temperature, *T*. This calculation is summarized Table 1 for 50 nm diameter nanoshells with a 7 nm wall thickness, then for several types of particles in Figure 8.

The TEM images (Fig. 5) and UV/Vis spectra (Fig. 4) provide clear evidence that the gold nanoshells melt and/or anneal in response to NIR pulsed laser irradiation in agreement with the calculations in Table 1 and Fig. 8. The nanoshells are not small enough to exhibit appreciable melting point depression as predicted via the Kelvin equation [54], hence the nanoshells must be adsorbing sufficient energy to reach the bulk melting point of gold (1064° C). From Table 1, and Figure 8, the largest gold nanoshells are estimated to reach temperatures of ~ 1700 - 1800 °C, while the smaller nanoshells may reach the vaporization point of gold. The diameter of the nanoshell determines the absorption and scattering at 800 nm for a given shell thickness (Fig. 7). However, the mass of gold in the nanoshell increases with the square of the nanoshell diameter, which means that the energy needed to heat the nanoshell also increases with the square of the nanoshell radius. Hence, the optimal nanoshell size for maximum temperature rise is not the same as for maximum total energy absorption or duration of energy absorption (Fig. 6). Fig. 8 shows the surprising result that the largest particles with the best overlap with the NIR laser actually have the smallest temperature rise, even though they adsorb the greatest fraction of the incident light energy. The results in Fig. 8 for the maximum nanoshell temperature assume that dissipation of heat to the surrounding solution is slow compared to the time for plasmonic heating and that all the absorbed energy goes into increasing the nanoshell temperature [16,23,43,44,47].

Figure 9 shows the measured temperature rise of 3 ml of suspension irradiated for 15 minutes with 680 μJ-pulse^{-1} 800 nm NIR light at 1 kHz (0.68 W net power). The initial heating rate is much larger than the rate after 15 minutes of irradiation, consistent with the increase in light transmission seen in Fig. 6 as the nanoshells melt, change shape, and the SPR resonance is blue shifted to the 500 - 600 nm resonance of solid spherical nanoparticles (Fig. 5). Most of the temperature rise occurs over the first minute or two, then the sample temperature reaches a steady state showing that the decreased energy input from adsorption is offset by losses from the suspension vial to the lab environment.

If all 0.68 W of light energy was absorbed by the solution, the maximum heating rate of 3 ml of water would be ~3.2 °C-min^{-1}; the initial heating rate of the largest nanoshells (.41 mmol Au) is ~ 2.5 °C-min^{-1} and decreases for the smaller nanoshells. The initial temperature increase of the solution, which is indicative of the total energy absorption of the nanoshells, increases with increasing nanoshell size (and overlap of the SPR peak with the excitation light). This order is reversed from the maximum temperature rise of the individual nanoshells (Fig. 8); the largest nanoshells are the most efficient energy absorbers, but have the smallest maximum temperature rise for the individual nanoshell (Fig. 8).

Fig. 6d shows that light absorption decreases significantly during the 10 minutes of irradiation (Fig 6d), eventually leading to a steady state temperature at which losses from the sample vials equals the net rate of energy absorption [43]. The steady state increase in temperature of the solution is proportional to the absorbance of the nanoparticles after the morphological and SPR resonance changes induced by the irradiation seen in Fig. 6d. The steady state temperature increases of the larger particles (3.2, 2.0 and 1.0 °C) are directly proportional to the gold

concentration in the suspension (.41 mmol, .24 mmol and .125 mmol). Although the individual nanoparticles are heated to melting after the morphological changes (See Fig. 8), the steady state solution temperature increase is only a few degrees above ambient. As soon as the irradiation ends, the suspension quickly goes back to room temperature.

Heating the solution a second time (Fig. 9b) shows that the time to reach steady state more than doubles for the 40 nm nanoshell suspension (0.25 mmol Au) than the first heating cycle. However, the steady state temperature increase was about 2° C for both cycles. This is consistent with the TEM images in Fig. 5 that shows that the nanoshells have been degraded during the first irradiation and that the steady state temperature increase is due to off-resonance heating of the melted and annealed nanoshells (Fig. 4). The differences in steady state temperature in Fig. 9a primarily result from the differences in gold concentration in the solution, rather than the initial size of the gold nanoshells. By the time the suspension has reached a steady temperature, all of the nanoshells have been melted and annealed into stable, spherical solid nanoparticles with an SPR peak at 500- 600 nm; only the total concentration of the melted nanoshells is different between the samples. Manipulating the particle morphologies to tune the SPR absorbance to the irradiation wavelength does not affect the steady state temperature of the suspensions when pulsed laser radiation is used. Similar on and off resonance heating of gold nanorods was also reported by Link et al[2,63].

4. Conclusions

The emphasis of the synthesis presented here is on the facile and scalable nature of a new reaction pathway to gold nanoshells that (1) eliminates separation and centrifugation steps; (2) has minimal heating or special environmental concerns; and (3) has no toxic reactants, additives or solvents. The fact that gold nanoshells with controlled size can be made rapidly and reproducibly via simple colloidal chemistry methods simplifies their use in applications ranging from biomedical imaging to Raman spectroscopy to catalysis. In particular, how these gold nanoshells respond to NIR laser irradiation is of crucial importance to understanding how to use them most efficiently.

The unexpected result of this study is that even nanoshells that have a SPR peak significantly removed from the 800 nm wavelength of the irradiating pulsed laser light can be heated to sufficiently high temperatures that they are quickly melted and annealed into more stable solid spherical nanoparticles. The energy absorbed by the nanoshells depends on the overlap between the SPR peak and the wavelength of the irradiation source, and hence on the diameter/shell thickness ratio. However, the maximum temperature of the nanoshells is limited by the mass of the nanoshells, which increases as the square of the diameter. Optimizing the nanoshell structure for maximum absorption of femtosecond NIR pulses does not necessarily provide the highest temperatures for the individual nanoshells during irradiation. For continuous wave laser irradiation, the nanoshell temperature does not increase significantly over the temperature of the solution as the energy input to the particle is dissipated quickly into the surrounding media [43,56]. The instantaneous continuous wave power input is of order 10^{10} lower than for femtosecond pulses, even though the average power input to the system is the same. Hence, maximum energy absorption is the only relevant feature for continuous wave heating, which has led to much of the effort to tailor nanoparticle structure to maximize absorption at the irradiation wavelength. However, it is not yet known if maximizing the nanoshell temperature or the energy absorption is more important for biomedical applications such as photothermal destruction of cancer or bacterial cells [3,6,7,16,23,47,55] with pulsed radiation. As all of the nanoshells anneal to form solid, spherical nanoparticles of 10 - 40 nm diameter with a common SPR peak from 500 -600 nm, the steady state temperature rise is governed only by the total gold concentration in the suspension, rather than the initial size and shape of the nanoshells.

5. Experimental

Nanoshell synthesis and characterization

Gold nanoshells were prepared by reducing gold tetrachloroauric acid ($HAuCl_4$) onto silver nanoparticle templates in a process adapted from Hao et al. [27]. Silver nanoparticles were prepared at 60°C in a well stirred solution of 0.2 mmol silver nitrate (50 mL, $AgNO_3$, Aldrich) in the presence of sodium citrate (0.5mmol) following an injection of 100 mmol sodium borohydride solution (1 mL, $NaBH_4$, Aldrich) which produces a characteristic yellow color. The silver sols were allowed to stir at 60°C for a minimum of two hours. After cooling to room temperature, larger silver nanoparticles could be grown from these stock sols, if desired. Silver particle growth was initiated by adding a 200 mmol hydroxylamine hydrochloride solution (1mL, $NH_2OH \bullet HCl$, Aldrich) to the silver sol followed by stirring for five minutes [51-54], followed by addition of of 0.1 M $AgNO_3$ (0 - 1 mL). The growing silver nanoparticles turned the sol a darker yellow or orange depending on the amount of additional $AgNO_3$. After stirring for a minimum of two hours (and often aging overnight), gold nanoshells were made via galvanic replacement chemistry from the template silver sols. First, a given silver sol (50 mL) was heated to 60°C and the necessary amount (100 - 500 μl) of 25 mmol tetrachloroauric acid ($HAuCl_4$, Aldrich) were added dropwise (depending on the initial silver template size). The reactions were monitored using UV/vis/NIR spectroscopy, and stopped when the silver peak located near 400 nm vanished, which occurred when the gold/silver ratio in the reaction vessel approached the stoichiometric ratio of 1:3 (to err on the side of completion, the ratio was usually .37:1). Once the reaction was complete, the samples were cooled, silver chloride was allowed to precipitate, and the supernatant containing the gold nanoshells was transferred to another vessel and stored at 4°C until further use.

Nanoparticle concentrations were ~ 10^{10} - 10^{11} mL^{-1}, based on the average dimensions measured using transmission electron microscopy (TEM) and the known amounts of materials used during the reaction. For TEM, approximately 2 μL samples of nanoshell suspensions were spread onto formvar-coated TEM grids (Ted Pella, Redding, California) and dried in vacuum. Digital TEM micrographs were obtained using an FEI Technai Sphera TEM (FEI, Netherlands) equipped with a CCD camera (Gatan, Pleasanton, Ca) operating in transmission mode at 200 keV. X-ray photoelectron spectroscopy (XPS) using a Kratos Axis Ultra instrument was used to map the relative composition of nanoshells after galvanic replacement chemistry.

Laser irradiation

The particle suspensions were irradiated with a Ti:Sapphire laser (Spectraphysics Spitfire) that generates 90 fs pulses at a 1 kHz repetition rate with energies up to 800 $\mu Jpulse^{-1}$. The energy incident on the samples was varied using neutral density filters. The Gaussian width of the beam was 2.3 mm (area of .042 cm^2). Typically, 3 mL of the sample was irradiated in a quartz cell with a 1-cm path length. Samples were irradiated for 10 - 15 minutes, and the transmitted intensity was measured with a power meter. This irradiation time was sufficient for the measured transmitted intensity to reach a steady value. A Teflon stir-disk was placed at the bottom of the cell to ensure good mixing. The cell was placed atop a magnetic stir-plate (housed within a ceramic holder with four openings on its sides to insulate the cell and hold it steady). To insulate the cell during irradiation, the base of the holder rested on 0.3 cm thick foam (to minimize heating due to the stirrer motor); to prevent evaporation, the cell was capped.

Calorimetry

The temperature of the particle suspensions in the irradiation cell was measured using a .0625 inch thick stainless steel K-type thermocouple probe (Omega Engineering, Inc., Stamford, CN) inserted through the plastic cap into the top few millimeters of fluid (well away from the laser path). The thermocouple was linked to an Omegaette HH306 digital thermometer (Omega)

that was interfaced to a computer using Thermolog data acquisition software (Omega). The extinction (absorbance) spectra of the samples before and after irradiation were measured with the UV-vis spectrophotometer. After irradiation, each sample was imaged with TEM as described previously.

6. Acknowledgements

NSF Grant CTS-0436124 and a NIH Program of Excellence in Nanotechnology Grant HL080718: *Nanotherapy for Vulnerable Plaques,* supported this work.

7. References

1. Weissleder R. Nature Biotechnology 2001;19:316–317.
2. Link S, Burda C, Nikoobakht B, El-Sayed MA. Chem. Phys. Letters 1999;315:12–18.
3. Hirsch LR, Stafford RJ, Bankson JA, Sershen SR, Rivera B, Price RE, Hazle JD, Halas NJ, West JL. PNAS 2003;100:13549–13554. [PubMed: 14597719]
4. Pham T, Jackson JB, Halas NJ, Lee TR. Langmuir 2002;18:4915–4920.
5. West JL, Halas NJ. Annual Review of Biomedical Engineering 2003;5:285–292.
6. O'Neal DP, Hirsch LR, Halas NJ, Payne JD, West JL. Cancer Letters 2004;209:171–176. [PubMed: 15159019]
7. Gobin AM, O'Neal DP, Watkins DM, Halas NJ, Drezek RA, West JL. Lasers in Surgery and Medicine 2005;37:123–129. [PubMed: 16047329]
8. Kalele SA, Kundu AA, Gosavi SW, Deobagkar DN, Deobagkar DD, Kulkarni SK. Small 2006;2:335–338. [PubMed: 17193045]
9. Moghimi SM, Hunter AC, Murray JC. FASEB Journal 2005;19:311–330. [PubMed: 15746175]
10. Pissuwan D, Valenzuela SM, Cortie MB. Trends in Biotechnology 2006;24:62–67. [PubMed: 16380179]
11. Zweifel DA, Wei A. Chem. Mater 2005;17:4256–4261. [PubMed: 17415410]
12. Chen JY, Wang D, Xi J, Au L, Siekkinen A, Warsen A, Zhi-Yuan L, Zhang H, Xia YN, Li X. Nano Letters 2007;7:1318–1322. [PubMed: 17430005]
13. Norman RS, Stone JW, Gole A, Murphy CJ, Sabo-Attwood TL. Nano Letters 2008;8:302–306. [PubMed: 18062714]
14. Conner EE, WMwamuka J, Gole A, Murphy CJ, Wyatt MD. Small 2005;3:325–327.
15. Lapotko DO, Lukianova E, Oraevsky A, A. Lasers in Surgery and Medicine 2006;38:631–42. [PubMed: 16736503]
16. Zharov VP, Mercer KE, Galitovskaya EN, Smeltzer MS. Biophys. J 2006;90:619–627. [PubMed: 16239330]
17. Westcott SL, Oldenburg SJ, Lee TR, Halas NJ. Chemical Physics Letters 1999;300:651–655.
18. Averitt RD, Sarkar D, Halas NJ. Phys. Rev. Lett 1997;78:4217–4220.
19. Oldenburg SJ, Averitt RD, Westcott SL, Halas NJ. Chemical Physics Letters 1998;288:243–247.
20. Sershen SR, Westcott SL, Halas NJ, West JL. Journal of Biomedical Materials Research 2000;51:293–298. [PubMed: 10880069]
21. Hirsch LR, Gobin AM, Lowery AR, Tam F, Drezek RA, Halas NJ, West JL. Ann. Biomed. Eng 2006;34:15–22. [PubMed: 16528617]
22. Cui JQ, Kretzschmar I. Langmuir 2006;26:8281–8284. [PubMed: 16981737]
23. Prasad V, Mikhailovsky A, Zasadzinski JA. Langmuir 2005;21:7528–7532. [PubMed: 16042490]
24. Shi W, Sahoo Y, Swihart MT, Prasad PN. Langmuir 2005;21:1610–1617. [PubMed: 15697315]
25. Sun YG, Mayers BT, Xia YN. Nano Letters 2002;2:481–485.
26. Sun YG, Xia YA. Nano Letters 2003;3:1569–1572.
27. Hao E, Li SY, Bailey RC, Zou SL, Schatz GC, Hupp JT. J. Phys. Chem. B 2004;108:1224–1229.
28. Wiley B, Herricks T, Sun YG, Xia YN. Nano Letters 2004;4:1733–1739.
29. Wiley B, Sun YG, Chen JY, Cang H, Li ZY, Li XD, Xia YN. MRS Bulletin 2005;30:356–361.

30. Chen JY, Wiley B, Li ZY, Campbell D, Saeki F, Cang H, Au L, Lee J, Li X, Xia Y. Adv. Mater 2005;17:2255–2261.
31. Harris N, Ford MJ, Cortie MB. J. Phys. Chem.B 2006;110:10701–10707. [PubMed: 16771316]
32. Kumar GVP, Shruthi S, Vibha B, Reddy BAA, Kundu TK, Narayana C. J. Phys. Chem. C 2007;111:4388–4392.
33. Liang HP, Wan LJ, Bai CL, Jiang L. J. Phys. Chem. B 2005;109:7795–7800. [PubMed: 16851906]
34. Schwartzberg AM, Oshiro TY, Zhang JZ, Huser T, Talley CE. Analytical Chemistry 2006;78:4732–4736. [PubMed: 16808490]
35. Jain PK, Lee KS, El-Sayed IH, El-Sayed MA. J. Phys. Chem.B 2006;110:7238–7248. [PubMed: 16599493]
36. Huang X, El-Sayed IH, Qian W, El-Sayed MA. J. Am. Chem. Soc 2006;128:2115–2120. [PubMed: 16464114]
37. Pissuwan D, Valenzuela SM, Miller CM, Cortie MB. Nano Letters 2007;7:3808–3812. [PubMed: 18034505]
38. Orendorff CJ, Sau TK, Murphy CJ. Small 2006;2:636–639. [PubMed: 17193100]
39. Novo C, Mulvaney P. Nano Letters 2007;7:520–524. [PubMed: 17298019]
40. Allen TM, Cullis PR. Science 2004;303:1818–1822. [PubMed: 15031496]
41. Hu M, Wang X, Hartland GV, Salgueirino-Maceira S, Liz-Marzan LM. Chem. Phys. Letters 2003;372:767–772.
42. Link S, Burda C, Nikoobakht B, El-Sayed MA. J. Phys. Chem. B 2000;104:6152–6163.
43. Roper DK, Ahn W, Hoepfer M. J. Phys. Chem. C 2007;111:3636–3641.
44. Ruan C-Y, Murooka Y, Raman RK, Murdick RA. Nano Letters 2007;7:1290–1296. [PubMed: 17397235]
45. Angelatos AS, Radt B, Caruso F. J. Phys. Chem. B 2005;109:3071–3076. [PubMed: 16851322]
46. Skirtach AG, Dejugnat C, Braun D, Susha AS, Rogach AL, Parak WJ, Mohwald H, Sukhorukov GB. Nano Letters 2005;5:1371–1377. [PubMed: 16178241]
47. Zharov VP, Letfullin RR, Galitovskaya EN. J. Phys. D: Appl. Phys 2005;38:2571–2581.
48. Oldenburg SJ, Jackson JB, Westcott SL, Halas NJ. Applied Physics Letters 1999;75:2897–2899.
49. Sershen SR, Westcott SL, West JL, Halas NJ. Applied Physics B-Lasers and Optics 2001;73:379–381.
50. Sun YG, Xia YN. J. Am. Chem. Soc 2004;126:3892–3901. [PubMed: 15038743]
51. Turkevich J. Gold Bulletin 1985;18:86–91.
52. Turkevich J, Garton G, Stevenson PC. J. Colloid Interfac. Sci 1954;9:S26–S35.
53. Turkevich J, Stevenson PC, Hillier J. Discussions of the Faraday Society 1951;11:55–75.
54. Link S, El-Sayed MA. J. Phys. Chem. B 1999;103:4212–4217.
55. Lin CP, Kelly MW, Sibayan SAB, Latina MA, Anderson RR. IEEE J. Sel 1999;5:963–968.
56. Richardson HH, Hickman ZN, Govorov AO, Thomas AC, Zhang W, Kordesch ME. Nano Letters 2006;6:783–788. [PubMed: 16608284]
57. Blatchford CG, Campbell JR, Creighton JA. Surface Science 1982;120:435–455.
58. Creighton JA, Blatchford CG, Albrecht MG. J. Chem. Soc. Faraday Trans. II 1979;75:790–798.
59. Hermans MH. Am. J. Nurs 2006;106:60–68. [PubMed: 17133010]
60. Kerker M. J. Colloid Interfac. Sci 1985;105:297–314.
61. Eckstein H, Kreibig U. Zeitschrift Phys. D - atoms, molecules and clusters 1993;26:239–241.
62. Buffat P, Borel J-P. Phys. Rev. A 1976;13:2287–2298.
63. Link S, Burda C, Mohamed MB, Nikoobakht B, El-Sayed MA. Phys. Rev. B 2000;61:6086–6090.

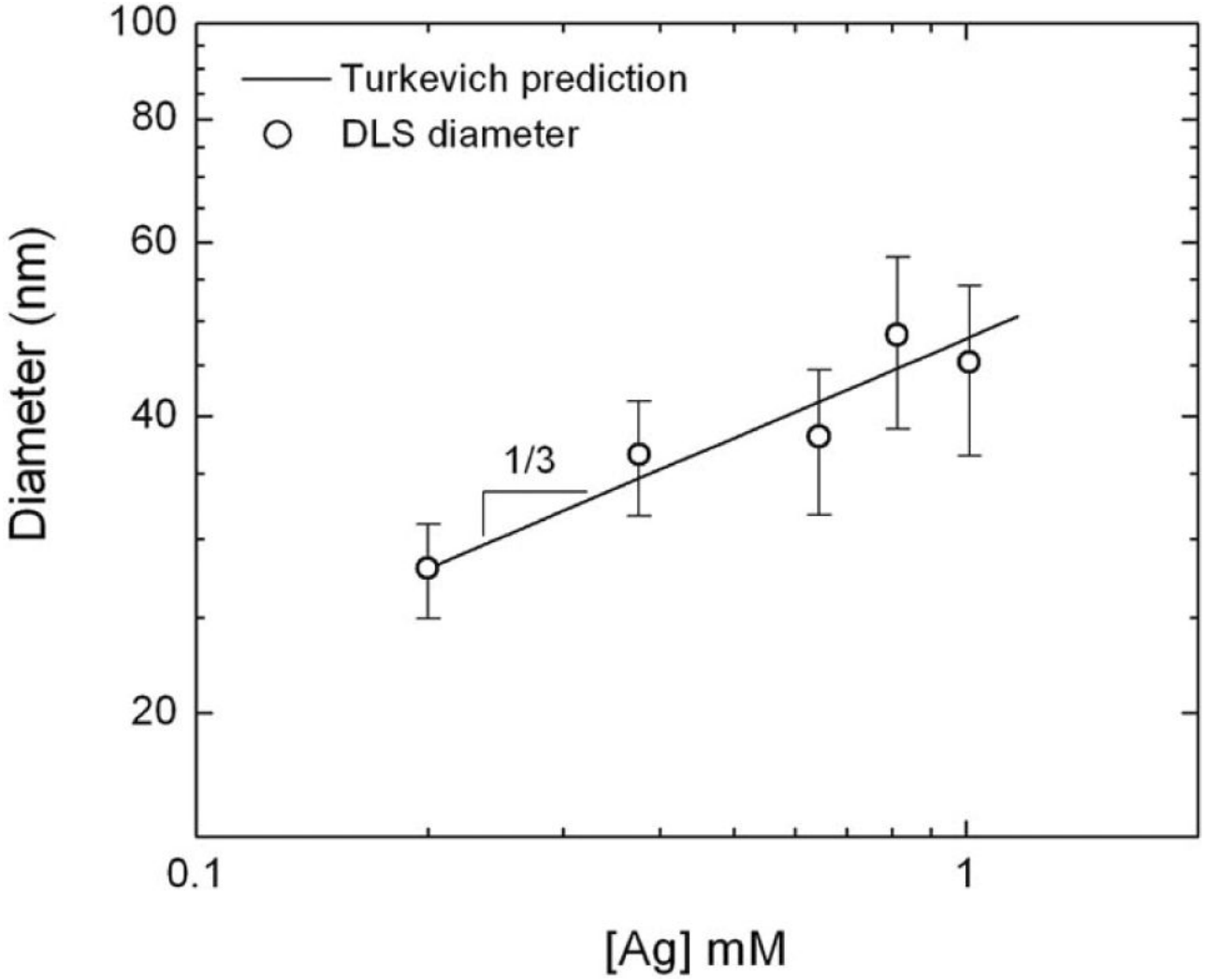

Figure 1.
Dynamic light scattering (DLS) measured diameters of the stock silver sol (0.2 mmol Ag) and the growth sols. The growth sol diameter scaled with the 1/3 power of the silver concentration confirming that all of the silver added to existing nanoparticles and did not nucleate new particles [51-53].

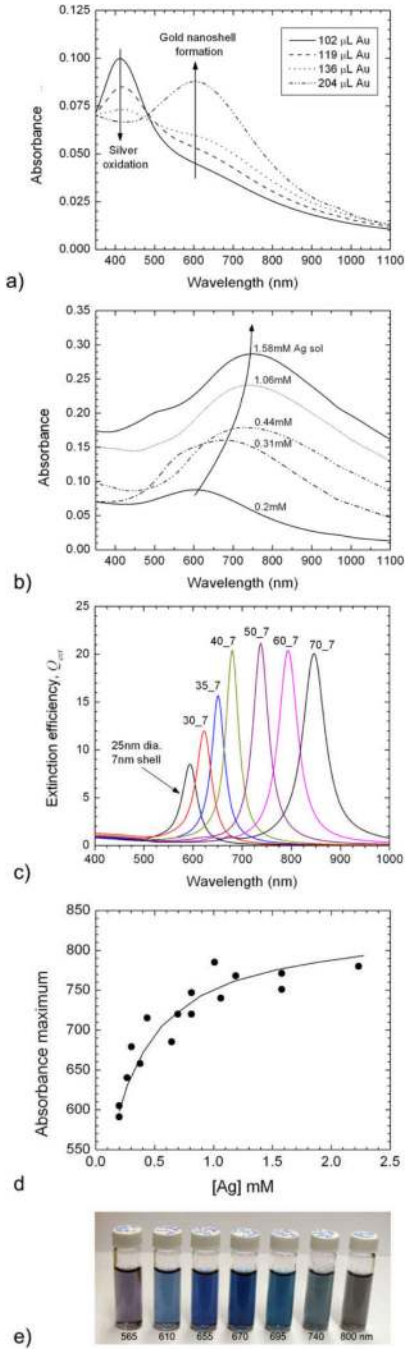

Figure 2.

(a) Ultraviolet/visible light spectrophotometry of the conversion of a 0.2 mmol Ag sol to a 0.09 mmol Au nanoshell suspension by adding increasing amounts of 25 mmol $HAuCl_4$. For clarity only four curves are shown.

(b) The resulting final absorbance spectra for gold nanoshells made from different sized silver sols (denoted by their initial silver concentration) after 10-fold dilution. The higher the silver concentration, the larger the silver template and the further red-shifted are the final gold nanoshells.

(c) Calculated extinction efficiencies for different sizes of gold nanoshells with a water core and water surroundings. The first number is the overall diameter of the nanoshell and the second

number is the shell thickness (i.e., 30_7 means a nanoshell of 30 nm diameter with a 7 nm shell). Increasing the nanoshell diameter for a given shell thickness shifts the surface plasmon resonance to longer wavelengths and increases the extinction efficiency.
(d) A summary of the dependence that the final gold nanoshell SPR has on the initial sacrificial silver sol (size and concentration). Each silver template started from a stock 0.2 mmol silver sol, and was grown from that to larger particles by adding more $AgNO_3$. The error in each point (sample to sample variation) is on the order of ± 15 nm (primarily due to the polydispersity in the initial silver template), but they are omitted for clarity. The curve is a guide the eye.
(e) A collection of different aqueous gold nanoshell dispersions prepared from silver sols of increasing concentration and particle size (from left to right). The average SPR absorbance maximum for a given sol is listed beneath each vial. The overall wavelength range is from ~ 560 - 800 nm, showing that the absorbance profiles of gold nanoshells made via galvanic replacement chemistry can be tuned across the NIR window.

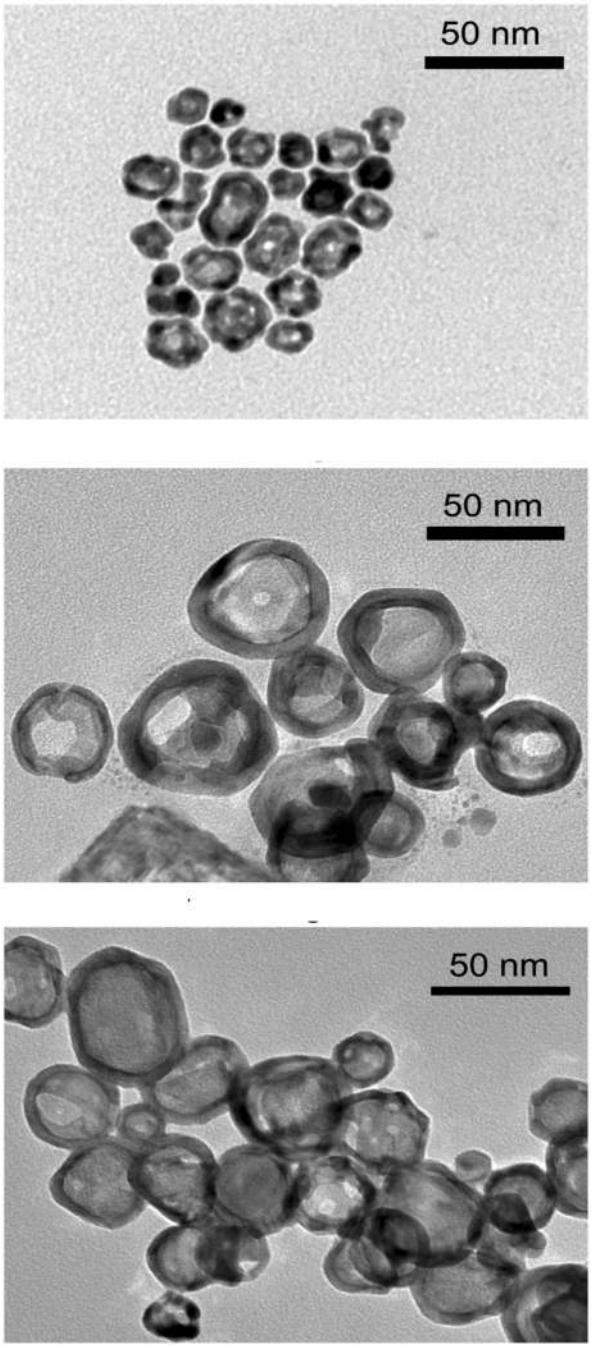

Figure 3.
TEM images of gold nanoshells made from the unmodified ~20 nm Ag sol (0.2 mmol Ag) and those made from the growth sol in which the concentration of silver was increased. Top: Unmodified 0.2 mmol Ag sol. Center: 0.304 mmol Ag. Bottom: 0.391 mmol Ag. The gold nanoshell size depends on the size of the sacrificial silver template. The center of each nanoshell is relatively electron-transparent, indicative of a hollow center showing that the silver template nanoparticle was converted to molecular silver.

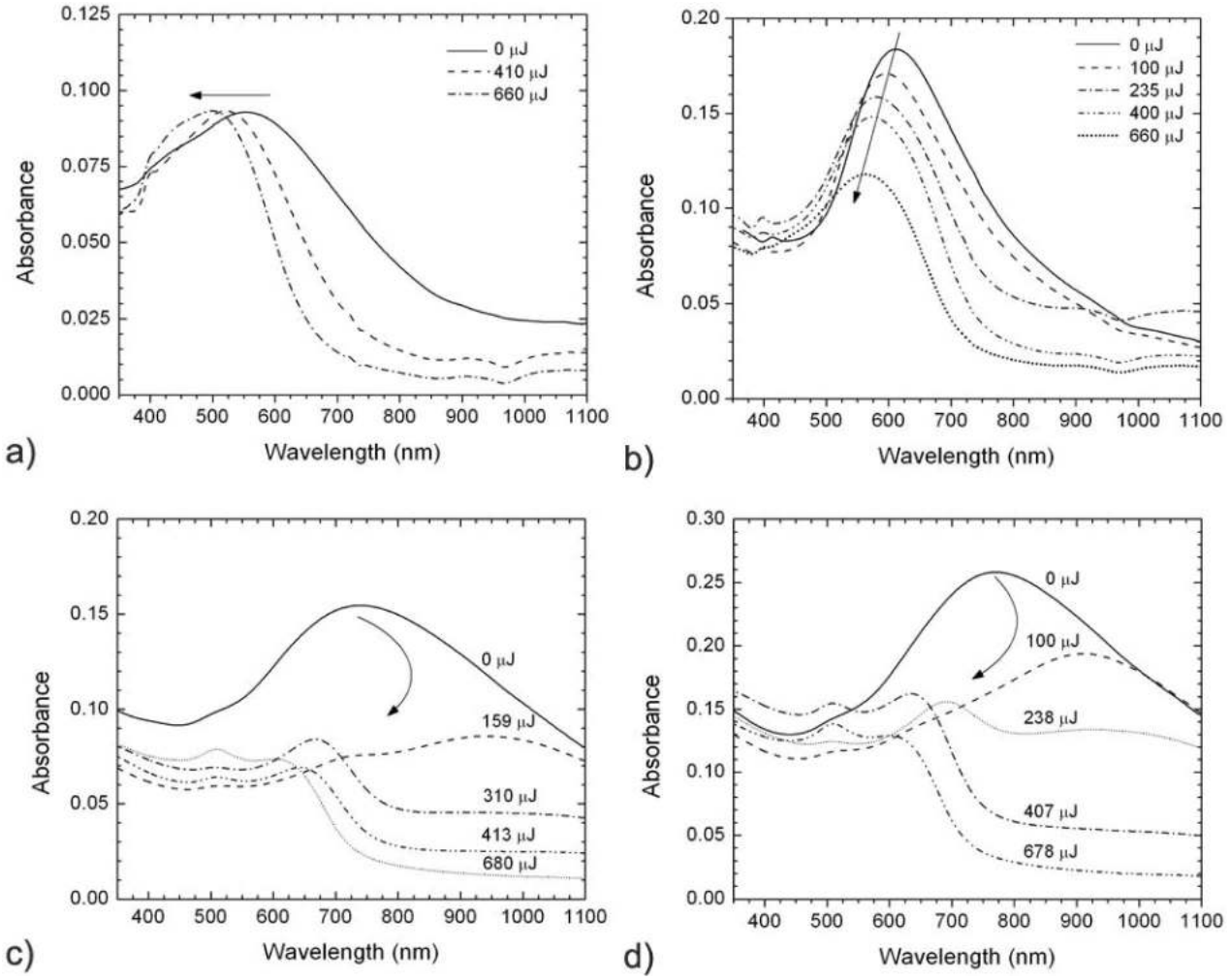

Figure 4.

UV/visible light spectra for different gold nanoshells suspensions after 10 minutes of exposure to 800 nm pulsed laser irradiation. (a) 0.09 mmol Au gold nanoshells from an initial 0.2 mmol Ag sol, (20 nm diameter, surface plasmon resonance, SPR ~ 600nm), (b) 0.124 mmol Au gold nanoshells from a 0.304 mmol Ag sol (30 nm diameter, SPR ~ 650 nm), (c) 0.25 mmol Au gold nanoshells from a 0.675 mmol Ag sol (40 nm diameter, SPR ~ 720 nm), and (d) 0.41 mmol Au gold nanoshells from a 1.07 mmol Ag sol (50 nm diameter, SPR ~ 750 nm). The arrows are in the direction of increasing laser power. A fresh, un-irradiated sample was used in each trial. The absorbance increases (from a-d) with increasing gold/silver concentrations as expected from Figs. 2 and 3; the higher concentrations lead to larger gold nanoshells with the surface plasmon resonance closer to the 800 nm irradiation wavelength. After 10 minutes of irradiation, all samples show a peak from 500 - 600 nm consistent with the formation of solid, spherical nanoparticles as seen in Fig. 5.

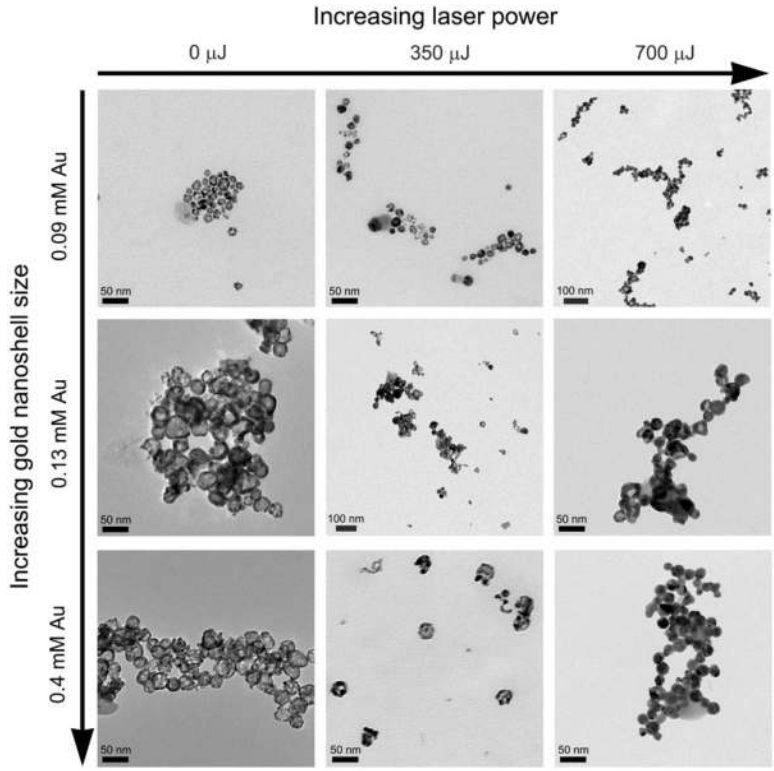

Figure 5.

TEM images of three different concentrations, 0.09 mmol, 0.13 mmol, and .41 mmol Au nanoshells before and after 10 minutes of irradiation with 800 nm light pulses of 350 or 700 μJ total energy. After irradiation with the higher energy pulses, all of the nanoshells have sintered and annealed resulting in 10 - 40 nm diameter solid spheres; the larger nanoshells anneal into larger spherical particles. At 350 μJ, the smaller particles from the 0.09 mmol sol have converted to the smaller diameter solid spheres. However, the larger particles from the 0.13 and 0.41 mmol sols first break apart upon absorbing the lower photon energy, leading to a disperse collection of asymmetric incomplete shells, oblate spheroids, rods and branched structures. The optical holes seen in Figs. 4c,d may be the result of these particle shapes that exhibit SPR shifted to longer wavelengths.

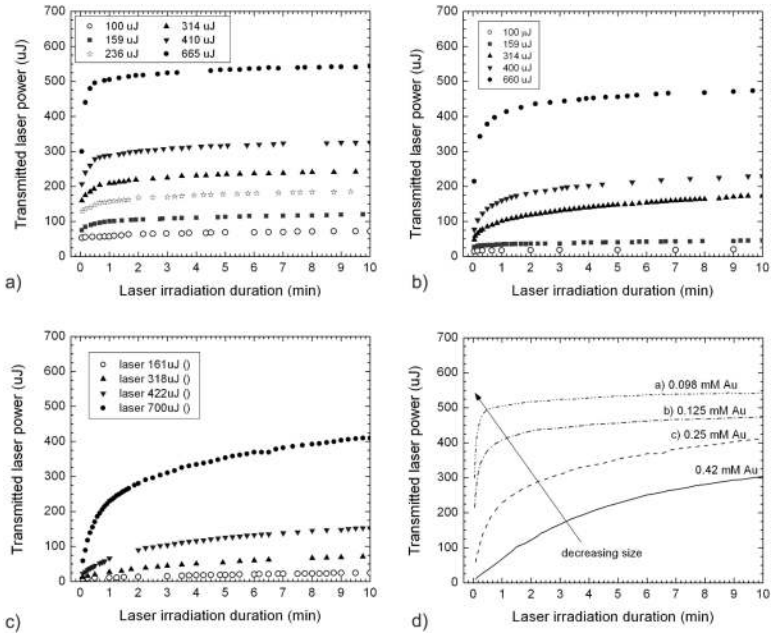

Figure 6.

Laser light transmission as a function of irradiation time for varying sizes of gold nanoshells: (a) 20 nm diameter (0.098 mmol Au), (b) 30 nm (0.125 mmol Au), (c) 40 nm (.25 mmol Au). The initial transmitted intensity is highest for the smallest nanoshells, consistent with the smallest overlap of the SPR peak (Fig. 2) with the 800 nm wavelength of the laser light. The transmitted intensity increases with time as expected from the spectra in Fig. 4 that show the nanoshells eventually are melted and annealed into solid spherical nanoparticles with less absorption at 800 nm (Fig. 4)

(d) Highest (700 μJ-pulse^{-1}) energy laser absorbance kinetics comparison for the nanoshells in (a), (b), (c) and for ~ 50 nm diameter gold nanoshells (0.42 mmol Au). The larger nanoshells anneal much more slowly than the smaller nanoshells, resulting in lower light transmission after 15 minutes.

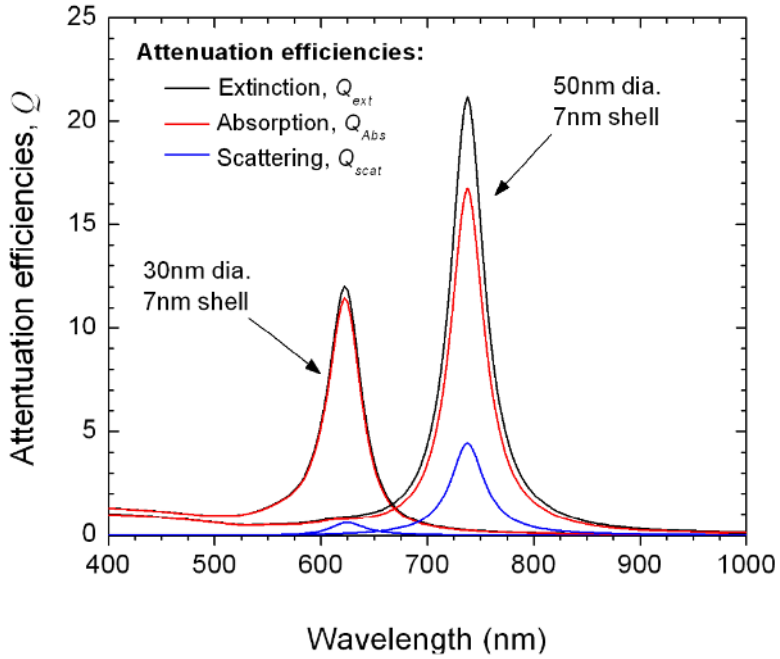

Figure 7.

Mie calculations of the relationship between scattering (blue curves), absorption (red curves) and total extinction (black curves) as a function of particle size. The larger particles scatter a larger fraction of the light and hence are less efficient absorbers, although the wavelength of the peak absorption overlaps more strongly with the excitation wavelength (800 nm) of the incident NIR radiation. The relative adsorption efficiency (ε_A in Eqn. 2) is the ratio of the absorption to the total extinction and is ~0.95 for the 30 nm nanoshells and ~0.8 for the 50 nm diameter nanoshells.

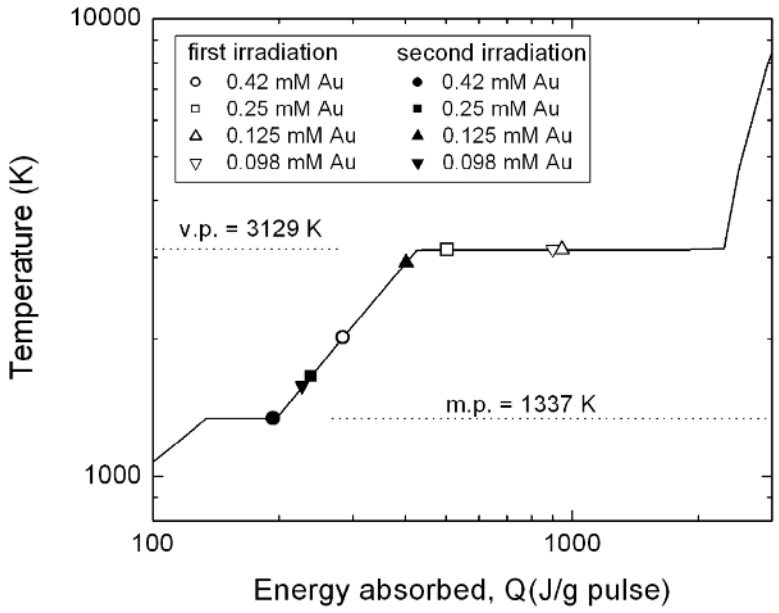

Figure 8.

Estimate of maximum nanoshell temperature upon initial irradiation (open symbols) and after 10 minutes irradiation (closed symbols) with maximum laser power (~690μJ-pulse^{-1}) using Eqns. 2, 3 and total extinction determined from Fig. 6 and efficiencies from Fig. 7. The different concentrations correspond to different nanoshell diameters: 0.098 mmol Au: 20 nm, 0.125 mmol Au : 30 nm, 0.25 mmol Au : 40 nm, and 0.42 mmol Au : 50 nm. While the extinction peak for the smaller nanoshells (lower Au concentrations) does not overlap with the incident laser wavelength as well as that for the larger nanoshells (Fig. 7), the proportionately greater increase in mass of the larger nanoshells leads to a smaller increase in the maximum temperature.

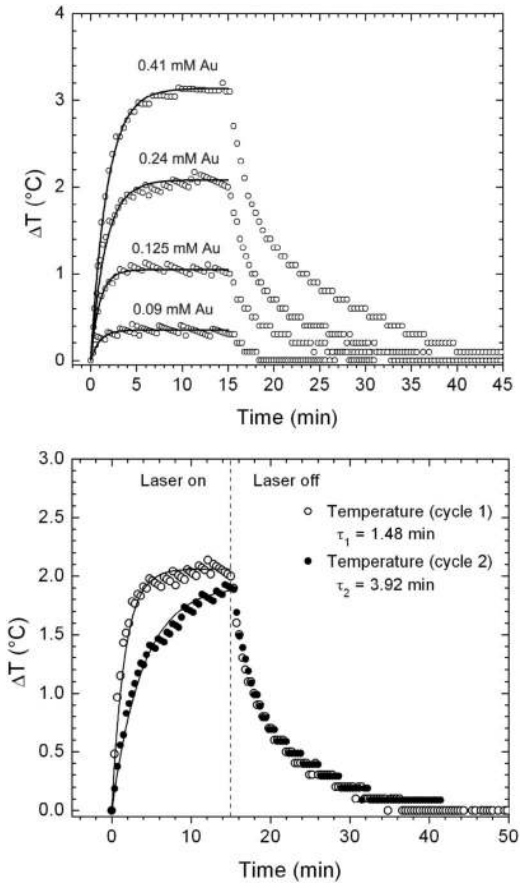

Figure 9a.

Experimental calorimetric data showing the degree of heating due to different 3 ml totl volume gold nanoshell suspensions after being irradiated for 15 minutes with 680 uJ-pulse^{-1} energy at 1 kHz (.68 W net power). These decreasing concentration of gold correspond to (a) ~ 20 nm, (b) ~ 30 nm, (c) ~ 40 nm, and (d) ~ 50 nm nanoshells. The largest particles adsorb the largest total energy as shown by the net increase in water temperature. The steady state increase in temperature for the nanoshells scales roughly with the gold mass ratio for the larger nanoparticles; the .24 mmol nanoshell suspension temperature increase is roughly twice that (2 °C vs 1 °C) of the .125 mmol nanoshell suspension.

(b) Calorimetry of resonance and off resonance heating via laser absorption for the a nanoshell suspension which had an initial SPR of ~ 750 nm (open circles), and after melting was subsequently cooled and then irradiated again (closed circles). The initial rise in temperature is much faster for the first irradiation, but levels off to roughly the same steady state temperature as the second irradiation. This is because the nanoshells are being transformed during the first irradiation to smaller, solid gold nanoparticles (Fig. 5, 6) that adsorb less light energy. By the time steady state is reached, most of the nanoshells have been converted to nanoparticles with a SPR from 500-600 nm (Figs. 4,5). These smaller nanoparticles also absorb laser energy, just with much less efficiency.

Table 1

A comparison of calculated temperatures attained by the gold nanoshells due to plasmonic heating (for the same concentration of gold, 41.4 g/m^3). The change in morphology after irradiation causes a drastic drop in the absorbance of the 800 nm wavelength light from a Ti:Sapphire laser (pulse duration = 90 fs, repetition rate = 1kHz).

Duration of laser Irradiation	Laser energy I_0 (μJ-pulse^{-1})	Particle morphology	*A*, gold sol absorbance	ε_A, scattering efficiency	Absorbed energy Q_{abs} (J-gram^{-1})	*T*, final (°C)
Initial, t = 0	680	~ 50nm core, 7nm thick	2.49	~ 0.8	284	1723
after 10 min.	680	~ 30nm solid particle	0.37	~ 0.98	193	1064